Gd III and Ga III complexes with a new tris-3,4-HOPO ligand as new imaging probes: complex stability, magnetic properties and biodistribution

Silvia Chaves, Karolina Gwizdala, Karam Chand, Lurdes Gano, Agnes A. Pallier, Éva Tóth, M. Amélia Santos

ARTICLE

Gd^{III} and Ga^{III} complexes with a new tris-3,4-HOPO ligand towards new imaging probes: complex stability, magnetic properties and biodistribution

Received 00th January 2022,
Accepted 00th January 2022

DOI: 10.1039/x0xx00000x

Silvia Chaves,[a] Karolina Gwizdała,[a,b] Karam Chand,[a] Lurdes Gano,[c] Agnès Pallier,[d] Éva Tóth[d] and M. Amélia Santos*[,a]

The development of metal-based multimodal imaging probes is a highly chalenging field in coordination chemistry. In this context, we have developed a bifunctonal hexadentate tripodal ligand (H_3**L2**), with three 3,4-HOPO moieties attached to a flexible tetrahedral carbon bearing a functionalizable nitro group. Complexes formed with different metal ions have potential interest for diagnostic applications, namely for magnetic resonance imaging (MRI) and positron emission tomography (PET). Its capacity to coordinate Gd^{III} and Ga^{III} was studied and the thermodynamic stability constants of the respective complexes were determined by potentiometry and spectrophotometry. The ligand forms stable 1:1 ML complexes though with considerably higher affinity for Ga^{III} than for Gd^{III} (pGa = 26.2 and pGd = 14.3 at pH 7). Molecular dynamics simulations on the Gd^{III} complex indicate that two water molecules can coordinate the metal ion, thus providing efficient paramagnetic enhancement of water proton relaxation. The relaxation and the water exchange properties of the Gd^{III} chelate, assessed by a combined ^{17}O NMR and ^{1}H NMRD study, showed associatvely activated water exchange witha relatively low rate constant, k_{ex}^{298} = (0.82±0.11)×10^7 s^{-1} and some aggregation tendency. Biodistribution studies of the ^{67}Ga-**L2** complex suggested good *in vivo* stability and its quick renal clearance. Further anchoring of this ligand with specific biotargeting moieties might open future prospectives for the applications of the labelled conjugates in both MRI or ^{68}Ga-PET diagnostic imaging.

Introduction

Among modern diagnostic and molecular procedures used for the visualization of diverse biological mechanisms occurring at cellular and molecular levels, magnetic resonance imaging (MRI) is one of the most powerful techniques due to its excellent spatial and temporal resolution in deep tissues. In some applications, the complementation with other diagnostic modalities providing different sensitivity or resolution, such as the screening of cancer-specific tissues, is of primordial importance, and nuclear imaging such as positron emission tomography (PET) or single photon emission computed tomography (SPECT) is particularly important. The development of imaging probes easily adaptable to either of the two imaging modalities, for instance by simply changing the metal ion, has attracted considerable attention, and the chemical design of ligands for such multiple imaging applications is a challenging area in coordination chemistry.[1]

The most commonly used ^{1}H-MRI contrast agents (CAs) are paramagnetic Gd^{III}-based complexes, due to the high electron spin and slow electronic relaxation of Gd^{III}. Besides high relaxivity, Gd^{III}-based CAs need to have high thermodynamic stability and kinetic inertness to avoid toxicity resulting from transmetalation assisted by endogenous metal ions (Cu^{II}, Zn^{II}) or ligands. Despite the very active research on MRI CAs,[2] clinical CAs are all Gd^{III} complexes of macrocyclic or open-chain poly(amino-carboxylate) ligands, such as 1,4,7,10-tetra-azacyclododecane-1,4,7,10-tetraacetic acid (H_4DOTA) or diethylene-triamine pentaacetic acid (H_5DTPA), and most of the complexes investigated in the context of MRI involve derivatives of these ligands, including conjugates with different bio-vectors.[3] Their MRI efficacy is mainly determined by the longitudinal relaxivity, r_1, which depends on several microscopic characteristics of the complexes. These include the number and the exchange rate of the water molecules in the inner coordination sphere of the Gd^{III} (q and k_{ex}), the rotational correlation time (τ_R) of the complex and the electron spin relaxation times of Gd^{III} ($T_{1,2e}$).

Concerning metal-based PET radiocomplexes, $^{68}Ga^{III}$ chelates are attractive because of the short half-life (1.1 h) and easy availability of the ^{68}Ga isotope from a $^{68}Ge/^{68}Ga$ generator.[4]

[a] Centro de Química Estrutural, Institute of Molecular Sciences, Departamento de Engenharia Química, Instituto Superior Técnico, Universidade de Lisboa, Av. Rovisco Pais 1, 1049-001, Lisboa, Portugal.
[b] Faculty of Chemistry, Gdansk University of Technology, Gabriela Narutowicza 11/12, 80-233 Gdansk, Poland.
[c] Centro de Ciências e Tecnologias Nucleares (C2TN), Instituto Superior Técnico, Universidade de Lisboa, Estrada Nacional 10, 2695-066 Bobadela LRS, Portugal.
[d] Centre de Biophysique Moléculaire, CNRS UPR 4301, Université d'Orléans, rue Charles Sadron, 45071 Orléans, France.
Electronic Supplementary Information (ESI) available: See DOI: 10.1039/x0xx00000x

^{68}Ga complexes with DOTA and DTPA-type ligands have been widely investigated, namely when bi-functionalized with diverse biological targeting moieties.[5]

For both MRI and PET imaging agents, there is a clear interest in the design of novel ligands towards higher structural diversity and in the characterization of their corresponding coordination complexes. For Gd^{III} complexes, one of the challenges is the increase of relaxivity via bishydration of the metal, while keeping good complex stability. As for Ga^{III}-based PET probes, in addition to high stability, the fast radiocomplex formation under mild conditions remains a key objective. In this aspect, acyclic ligands may have advantage over the macrocyclic ones, as evidenced by the currently most used PET radiotracer for prostate cancer, which is a ^{68}Ga complex with HBED-CC (*N*,*N*'-bis(2-hydroxy-5-(ethylenebetacarboxy)benzyl)ethylenediamine-*N*,*N*'-diacetic acid) extra-functionalized with a urea-based targeting moiety.[6]

Building on previous studies that demonstrated high relaxivity for HOPO-based Gd^{III} complexes in general,[7] and the interesting coordination properties of the hexadentate 3,4-HOPO-based-ligand (H_3L1) for Gd^{III} and Ga^{III},[8,9] we have decided to investigate a novel hexadentate ligand (H_3**L2**) and the physicochemical and biological properties associated with its complexes with these metal ions. Although both ligands contain three 3,4-HOPO moieties attached to an anchoring scaffold, in H_3**L2**, this moiety is a more flexible tetrahedral carbon, in contrast to the imino core of H_3**L1**. Furthermore, although neither of the ligands have biotargeting capacity, H_3**L2** bears an additional nitro group in the anchoring scaffold, which can be extra-functionalized with specific biotargeting moieties, and the bioconjugates labeled with metal tracers have potential in dual diagnostic applications, namely as MRI, or PET imaging agents. Examples of potential biotargeting moieties include cancer-targeting cyclic peptides (e.g. RGD or octreotide) or DUPA (2-[3-(1,3-dicarboxypropyl)-ureido]pentanedioic acid) to target a prostate specific membrane antigen (PSMA), which is overexpressed in prostate cancer.[10,11] It is noteworthy that the amine-bearing analogue of H_3**L2** (KC18) was recently studied in our group and demonstrated high chelating affinity towards Fe^{III} and Al^{III}, as well as good *in vivo* metal sequestration capacity.[12] Herein, besides the synthesis of the ligand H_3**L2**, we report its coordination capacity for Gd^{III} and Ga^{III} and the thermodynamic stability constants of the corresponding complexes, investigated by potentiometry and spectrophotometry. We have also assessed the relaxometric properties of the Gd^{III} complex by ^{17}O NMR and ^{1}H NMRD (Nuclear Magnetic Relaxation Dispersion) and carried out molecular simulations of the Gd^{III}-**L2** complex structure in order to support and rationalize the experimental results. Finally, *in vivo* studies have been performed by radiolabelling H_3**L2** with ^{67}Ga, a SPECT radionuclide used in nuclear medicine, and evaluating the biodistribution (gamma counting) of this radiotracer in mice.

Experimental

Synthesis of H_3L2

General synthetic information. All the chemicals (from Sigma-Aldrich or Acros) were of analytical reagent grade and, unless else specified, they were used without further purification**.** Whenever necessary, the solvents were dried according to standard methods.[13] All the reactions were TLC controlled, using aluminium plates coated with silica gel 60 F254 (Merck).

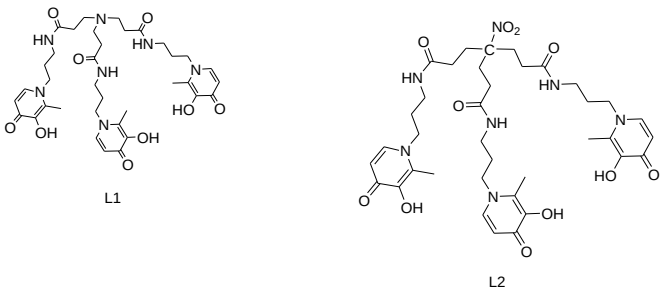

Fig. 1 Structural formulae of the hexadentate tripodal compounds H_3**L1** and H_3**L2**, symbolically abbreviated as **L1** and **L2**.

For column chromatography purifications was used silica gel 230–400 mesh (Geduran Si 60, Merck).

^{1}H and ^{13}C NMR spectra were performed in deuterated solvents (Methanol-d_4) at 25 °C, using Bruker AVANCE III 300 MHz spectrometers. The following abbreviations were used: s = singlet, d = doublet, t = triplet, p (pentet); m = multiplet. Melting points were measured with a Leica Galen III hot stage apparatus and are uncorrected. Mass spectra (ESI-MS) were obtained using a 500 MS LC Ion Trap (Varian Inc., Palo Alto, CA, USA) mass spectrometer equipped with an ESI ion source, operating in the positive or negative ion mode. For the target final compound, elemental analyses were performed using a Fisons EA1108 CHNS/O instrument at LAIST and were within the limit of ± 0.4%.

Synthetic procedure. The synthesis of the hexadentate 3-hydroxy-4-pyridinone derivative involved the coupling of nitromethanetrispropionic acid (**1**) with three amine-bearing 3-hydroxy-4-pyridinone arms, 1-(3-aminopropyl)-3-(benzyloxy)-2-methylpyridin-4(1H)-one (**2**), which was synthesized according to previously described.[8,14]

***N*^{1},*N*^{7}-Bis(3-(3-benzyloxy-2-methyl-4-oxopyridin-1(4*H*)-yl)propyl)-4-(3-(3-(3-benzyloxy-2-methyl-4-oxopyridin-1(4*H*)-yl)propylamino)-3-oxopropyl)-4-nitroheptanediamide (L2a)**

A solution of 1-(3-aminopropyl)-3-(benzyloxy)-2-methylpyridin-4(1*H*)-one **(2)** hydrochloride salt (0.986 g, 3.22 mmol) was previously neutralized with KOH (0.21 g, 3,86 mmol) in dry methanol (20 mL), and left stirring under nitrogen for 1.5 h. Then, the KCl precipitate, from the reaction mixture, was filtered off, the solvent was roto-evaporated and oily residue was dryed under high vacuum. Meanwhile, to a solution of nitromethanetrispropionic acid (**2**) (1.07 mmol) in dry DMF (25 mL), under N_2 atmosphere, was added *N*-methylmorpholine (4.29 mmol) and this mixture was left stirring for 10 min; afterwards, a DMF solution of propylphosphonic anhydride (T3P) (4.29 mmol) was dropwise added under nitrogen atmosphere and the reaction mixture was stirred for 30 min. Finally, a solution of the neutral 1-(3-aminopropyl)-3-(benzyloxy)-2-methylpyridin-4(1*H*)-one in dry DMF was added to the reaction mixture, which was then

left stirring at room temperature overnight, and the completion of the synthesis was confirmed by TLC. DMF of the reactional mixture was concentrated (up to 1/3 volume) by high vacuum distillation, and then the concentrated solution was taken in ethyl acetate and washed with brine solution. The organic phase was dried over anhydrous sodium sulphate, roto-evaporated and dried over vacuum. This crude material was purified through column chromatography over silica with 6% MeOH-DCM mixed eluent to afford the pure compound **L2a** (0.790 g, η = 71%), as white crystals, m.p. 94–96 °C. ^{1}H NMR (300 MHz, MeOD-d_4), δ (ppm): 7.74 (d, 3H, J = 6.0 Hz, 6-*H*Py), 7.32–7.40 (m, 15H, Ph), 6.51 (d, 3H, J = 9.0 Hz, 5-*H*Py), 5.08 (s, 6H, CH_2Ph), 4.00 (t, 6H, J = 7.5 Hz, CH_2CN), 3.19 (t, 6H, J = 7.5 Hz, CH_2CO), 2.19–2.23 (m, CH_2NH, CH_2NPy, CH_3), 1.83–1.88 (m, 6H, $CH_2CH_2CH_2$); *m/z* (ESI-MS): 1040.52 $(M + H)^+$.

***N*^{1},*N*^{7}-bis(3-(3-hydroxy-2-methyl-4-oxopyridin-1(4*H*)-yl)propyl)-4-(3-(3-(3-hydroxy-2-methyl-4-oxopyridin-1(4*H*)-yl)propylamino)-3-oxopropyl)-4-nitroheptanediamide (H_3L2)**

In a hydrogenation flask, the tris-(benzyloxi-3,4HP) intermediate **(L2a**) (0.769 g, 1 mmol) was dissolved in methanol (40 mL) and 10% Pd/C was added (0.21 g, 2 mmol); this suspension mixture was then shaked under a H_2 atmosphere (1 atm) for 4 h, at room temperature. Afterwards, the reactional suspension was filtered, the solvent was concentrated by rotoevaporation and the white solid precipitate was filtered and dried under vacuum line, affording the pure final product H_3**L2** (0.731 g, η = 95%); m. p. 126–128 °C. ^{1}H NMR (300 MHz, MeOD-d_4), δ (ppm): 7.67 (d, 3H, J = 6.0 Hz, 6-*H*Py), 6.43 (d, 3H, J = 9.0 Hz, 5-*H*Py), 4.10 (t, 6H, J = 7.5 Hz, CH_2CN), 3.27 (t, 6H, J = 6.0Hz, CH_2CO), 2.45 (s, 9H, CH_3), 2.27-2.20 (m, 12H; CH_2NH, CH_2NPy), 1.96 (p, 6H, J = 6.0 Hz, $CH_2CH_2CH_2$); ^{13}C NMR (75.5 MHz, MeOD-d_4), δ (ppm): 174.17, 170.18, 147.23, 138.94, 133.14, 112.71, 94.24, 53.11, 37.45, 31.88, 31.22, 31.07, 11.94; m/z (ESI-MS): 770.46 $(M+H)^+$); elemental analysis calc. for $C_{37}H_{51}N_7O_{11}$. 0.15 H_2O: C 57.52, H 6.69, N 12.69%; found: C 57.49, H 6.67, N 12.71%.

Metal complexation studies

Materials and equipment. The $GdCl_3$ (9.8×10^{-3} M) and $GaCl_3$ (4.2×10^{-3} M) stock solutions were prepared in HCl 0.1 M (to prevent hydrolysis) from the respective gadolinium and gallium salts and standardized by inductively coupled plasma emission (ICP). The 0.1 M HCl solution used in the calibration of the glass electrode was prepared from a Titrisol ampoule. The exact amount of HCl of the metal solutions was determined by the usual standard-addition method using 0.1 M HCl (Titrisol). The titrant solution used in pH-potentiometric and spectrophotometric titrations was prepared from a carbonate-free KOH commercial solution (Titrisol) and standardized by titration with a potassium hydrogen phtalate solution. This solution was discarded whenever the percentage of carbonate (Gran's method)[15] was higher than 1% of the total amount of base. The potentiometric studies were performed with an automated potentiometric apparatus containing a Crison micropH 2002 milivoltimeter, a Crison microBu 2031 burette and a Haake thermostatic bath (T = 25.0 ± 0.1 °C), controlled by PASAT program. Electronic spectra were recorded with a Perkin-Elmer Lambda 35 spectrophotometer, using 1 cm path length cells thermostated at 25.0 ± 0.1 °C.

Potentiometric measurements. Potentiometric titrations of the ligand H_3**L2**, alone or in the presence of the metal ions, were performed in water at ionic strength (I) 0,1 M KCl, T = 25.0 ±0.1 °C, by adding the KOH titrant. For all the samples prepared, the total volume was 20 mL, the ligand concentration (C_L) was 3.2×10^{-4} M and the metal ion to ligand molar ratios were 0:1 or 1:1. Each titration was performed 3-4 times and no solid phase was observed in the titrations of H_3**L2** alone, while for the titration of the M/H_3**L2** (M = Gd^{III}, Ga^{III}) systems some precipitation occurred above pH ca 7.

Spectrophotometric measurements. The electronic spectra of H_3**L2** and of the respective 1:1 Ga^{III}/H_3**L2** (C_L = 5.3×10^{-5} M) system were recorded in the wavelength range 250-400 nm, in aqueous solution (I = 0.1 M, KCl) and for pH > 2 and pH < 2. For pH > 2, the solutions of H_3**L2** and Ga^{III}/H_3**L2** system were prepared in a similar way to those used in potentiometry. Below pH 2, due to constraints in the working of the pH electrode, a batch titration has to be performed. So, the amount of acid to be added, from standard solutions (0.1 or 1 M, HCl), was calculated in order to adjust the pH and obtain specific pH values (0.8, 1, 1.2, 1.4, 1.6 and 1.8).

Calculation of equilibrium constants. The stepwise protonation constants, $K_i = [H_iL]/[H_{i-1}L][H]$, and the overall metal complex stability constants, $\beta(M_mH_hL_l) = [M_mH_hL_l]/[M]^m[H]^h[L]^l$, were determined with the Hyperquad 2008[16] and Psequad[17] programs by fitting, respectively, the potentiometric and spectrophotometric data. Errors were calculated by the program, after treating data corresponding to 3-4 titrations. The metal hydrolysis model was determined under the defined experimental conditions (I = 0.1 M KCl, T = 25.0 ± 0.1 °C) and the following values of stability constants were obtained: log β (GdH_{-2}) = -14.14 and log β (GdH_{-3}) = -21.03; log β (GaH_{-2}) = -7.05; log β (GaH_{-3}) = -10.42; log β (GaH_{-4}) = -14.82. The metal hydrolytic species, as well as the value of K_w ($10^{-13.96}$), were included in the equilibrium model. The species distribution curves were obtained with the Hyss program.[16]

MALDI-TOF measurements

The pH of the Gd^{III}/H_3**L2** and Ga^{III}/H_3**L2** (C_L = 6×10^{-5} M) systems in water was previously ascertained to 4.13 and 4.93 (C_L/C_{Gd} = 1) as well as to 3.04 and 4.18 (C_L/C_{Ga} = 1), by using KOH solution. Although different conditions/matrices were tried (CHCA, Dithranol, Laser Desorption Ionization - LDI) in positive and negative modes, signals for the complexes with the adequate isotopic distribution could only be found for the Ga^{III}/H_3**L2** system by using CHCA (α-cyano-4-hydroxycinnamic acid) matrix in positive mode. The MALDI-TOF mass measurements were performed by the RIAIDT-USC analytical lab (Universisty of Santiago de Compostela, Spain).

Molecular modeling

Molecular modeling studies were carried out aimed to provide some further insight into the molecular structure of Gd^{III}**L2** complex and, particularly, in the number of water molecules coordinated to the metal ion. These studies were performed with full geometry optimization of the gadolinium complexes by quantum mechanical calculations based on DFT methods included in the Gaussian 09 program software,[18,19] with the B3LYP hybrid functional[20] and the Stuttgart/Dresden ECP (SDD) basis set.[21] No symmetry constrains were enforced during geometry optimization. The calculations were also performed for one water molecule, by using the same functional and basis set. Concerning the Gd^{III}**L2** complexes, the electronic energies (E_{b1}) obtained at the PBE0/b1 level of theory were

converted to free energy (G_{b1}) at 298.15 K and 1 atm, by using zero point energy and thermal energy corrections based on structural and vibration frequency data calculated at the same level.

Water exchange rate and relaxometric properties of Gd^{III}L2

Relaxometric measurements. ^{1}H NMRD profiles of aqueous 0.49 mM Gd**L2** solution (pH = 6.2) were measured at 25 and 37 °C on a Stelar SMARTracer Fast Field Cycling NMR relaxometer (0.00024–0.24 T, 0.01–10 MHz ^{1}H Larmor frequency) and a Bruker WP80 NMR electromagnet adapted to variable-field measurements (0.47–1.88 T, 20–80 MHz), and controlled by the SMARTracer PC-NMR console. The temperature was controlled by a VTC91 temperature control unit and maintained by a gas flow. The temperature was determined according to previous calibration with a Pt resistance temperature probe. The Gd^{3+} concentration of the sample was verified by ICP-OES measurement.

^{17}O NMR studies. Variable-temperature ^{17}O NMR measurements of an aqueous solution of Gd^{III}**L2** complexes were performed on a Bruker Advanced 400 MHz spectrometer using a 10 mm BBFO probe (9.4 T, 54.2 MHz) in the temperature range 5–75 °C. The temperature was calculated according to published calibration routines with ethylene glycol and MeOH. Acidified water ($HClO_4$, pH 3.3) was used as diamagnetic reference. Transverse ^{17}O relaxation times were obtained by the Carl-Purcell-Meiboom-Gill spin-echo technique. To eliminate susceptibility corrections to the chemical shifts, the sample was placed in a glass sphere fixed in a 10 mm NMR tube. To improve sensitivity, $H_2{}^{17}O$ (10% $H_2{}^{17}O$, CortecNet) was added to achieve ~ 1% ^{17}O content in the sample. The pH of the sample was 6.3 and the Gd^{III}**L2** complex concentration was 0.45 mmol/kg.

Radiolabelling and Biodistribution studies

Radiolabelling of L2 with ^{67}Ga. To approximately 1 mg of ligand, dissolved in 500 µL of acetate buffer (0.4 M, pH ≈ 5), was added approximately 37 MBq of ^{67}Ga citrate (Curium, Netherlands B.V.) and incubated for 15 min at room temperature. Radiochemical purity was analyzed by ITLC using two chromatographic systems using a saline: acetic acid (9:1) mixture or just saline as eluents. After development, the radioactivity distribution in the ITLC strips was evaluated on a miniGita scanning device (Elysia Raytest). In the first system the ^{67}Ga-**L2** remains at R_f = 0 while the ^{67}Ga citrate migrates with R_f = 0.6–0.8. In saline, the ^{67}Ga-citrate remains at R_f = 0 while the ^{67}Ga-**L2** migrates to the solvent front.

Biodistribution studies. All animal experiments were performed in compliance with national and European regulations for animal care and ethics in animal experimentation. The biodistribution of the ^{67}Ga-**L2** was evaluated in groups of three female CD-1 mice (randomly bred, Charles River) weighting approximately 25–28 g each. Animals were injected intravenously with 100 µL (3.3–7.5 MBq/90–202 µCi) of the preparation via the tail vein. The animals were housed in a temperature- and humidity-controlled room with a 12 h light/12 h dark schedule and maintained on normal diet ad libitum. Mice were sacrificed by cervical dislocation at different time points (30 min, 1 h and 24 h) post-injection (p.i.). The injected radioactive dose and the radioactivity remaining in the animal after sacrifice were measured in a dose calibrator (Capintec). The difference between the radioactivity in the injected and sacrificed animal was assumed to be due to total excretion from whole animal body. Blood samples were taken by cardiac puncture at sacrifice. Then, tissue samples of the main organs were dissected, weighted and counted in a gamma counter (Berthold). Biodistribution results were expressed as percentage of the injected activity per gram tissue (% I.A./g).

Results and discussion

Synthetic chemistry

The hexadentate chelator tris-(3-hydroxy-4-pyridinone) or tris-3,4-HOPO, reported herein, was synthesized according to the procedure outlined in Scheme 1. The tripodal anchor (1) contains three carboxylic groups linked to a tetrahedral carbon atom and a free nitro group which can be used for further functionalization. Three amino-bearing 3-benzyloxy-4-pyridinone derivatives, 1-(3-aminopropyl)-3-(benzyloxy)-2-methylpyridin-4(1*H*)-one (2), synthesized as previously described,[8,12] were attached to the anchor structure by coupling the free amino group of the hydroxypyridinone arm to the carboxylic groups of the anchor, via amide group formation, to give the intermediate **L2a**. For this condensation, propylphosphonic anhydride (T3P) was used as carboxylic activating agent, resulting in a reaction with good yield (71%) and easy work-up. The final step was the deprotection (debenzylation) of the hydroxyl groups by catalytic hydrogenation under a moderate H_2 pressure to avoid further reactions, as the reduction of the nitro group.

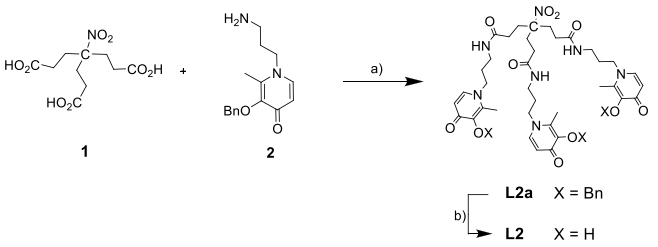

Scheme 1 Reagents and conditions: a) T3P, NMM, DMF, rt; b) H_2 (1 atm), Pd/C, MeOH. **L2** is a symbolic abbreviation for H_3**L2**.

Thermodynamics of metal complexation

The thermodynamic stability of the Gd^{III} and Ga^{III} complexes with the ligand H_3**L2** was evaluated by potentiometry and spectrophotometry, respectively. Firstly, the protonation constants of H_3**L2** were determined, and subsequently the global stability constants of the metal complexes were calculated by fitting the experimental data with the programs Hyperquad 2008 (potentiometric titrations)[16] or Psequad (spectrophotometric titrations),[17] taking into consideration the previously determined protonation constants as well as the metal hydrolysis species in the proposed models.

Acid-base properties of H_3L2. Potentiometric and spectrophotometric titrations of compound H_3**L2** were firstly performed in order to get the protonation constants required for the complexation model of the Gd^{III}/H_3**L2** and Ga^{III}/H_3**L2** systems, respectively. The potentiometric titration curve of

ligand H_3**L2** is presented in Fig. 2. The protonation constants, shown in Table 1, correspond to the average values of log K_i obtained through the fitting of the experimental potentiometric and spectrophotometric data.

Compound H_3**L2** has six dissociable protons (H_6L^{3+}) and the calculated stepwise constants for the protonation process are depicted in Table 1**.** Their assignment to the ligand basic centers is aided by previous studies of analogous tripodal 3,4-HP compounds such as H_3**L1,**[8,9,22] Kemp(PrHP)$_3$[23] or KC18.[14] Thus, the first three log K_i values correspond to the three hydroxyl groups and the last three values are relative to the pyridinium protons of the 3,4-HP units.

Apart from some small differences in acidity of the studied tripodal ligands, the six protonation constants found for H_3**L2** are analogous to those of Kemp(PrHP)$_3$ and Kemp(BuHP)$_3$, or to log K_i (i = 1–3, 5–7) for H_3**L1**. This is in accordance with the ligand structures where the corresponding protonation sites are quite far away from the anchoring skeleton, and the electron-donation effect from the homologous alkylic spacers should remain similar for the different ligands. Nevertheless, it can be detected that log K_4 = 4.26 and log K_5 = 3.11 for H_3**L2**,, which implies a difference of 1.15 log K values, while for the remaining compounds contained in Table 1 the corresponding difference is ca 0.67-0.73, more in agreement with the value 0.602 expected on a statistical basis for two equivalent basic groups.[24] Interestingly, the same difference in log K values (1.16) was found for KC21,[12] eventually arising from dissimilar stabilization in the arms through hydrogen bonds.

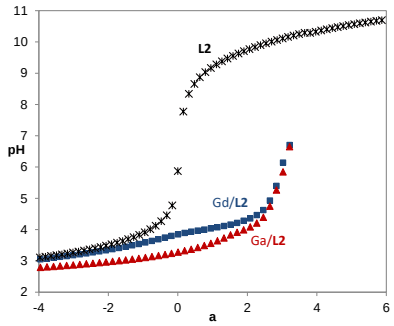

Fig. 2 Potentiometric titration curves for compound H_3**L2** and for the systems 1:1 Gd^{III}/H_3**L2** and 1:1 Ga^{III}/H_3**L2** ($C_L = 3.2 \times 10^{-4}$ M); a represents moles of added base per mole of ligand.

The species distribution diagram of H_3**L2** (see Fig. 3), as a function of pH and in the conditions of the spectrophotometric titrations, reveals that both protonated species, H_4L^+ and H_3L, have absorption maximum at 281 nm, while the deprotonated species (L^{3-}) absorbs at 312 nm. Moreover, for the pH range 4–9, the predominant species has neutral charge (H_3L). In particular, at physiological pH, H_3**L2** is mainly in the neutral form, (98% H_3L) and only 2% in the mono-negative species (H_2L^-).

Gd^{III} and Ga^{III} complexation. Fig. 2 shows the potentiometric titration curves obtained for the Gd^{III}/H_3**L2** and Ga^{III}/H_3**L2** systems in 1:1 stoichiometric condition, for which some precipitation occurred above pH ca 7 and therefore those experimental points were not considered while finding the corresponding complexation model. It is noticeable a change in the deprotonation profile of the H_3**L2** titration curve, due to the presence of the metal ions, in both M/L systems. The depicted potentiometric data was used to study the gadolinium complexation in solution, but the observed lower curve for the gallium system is merely indicative of the formation of a quite stronger gallium complex. In fact, gallium complex formation occurs below pH 2, thus the study of the Ga^{III}/H_3**L2** system needed to be performed by spectrophotometric titration.

The global stability constants determined by fitting analysis of the potentiometric (Gd^{III}/H_3**L2** system) and spectrophotometric titration data (Ga^{III}/H_3**L2** system, for 2< pH ≤ 2 assays, see Fig. S1) are shown in Table 1. For both systems the complexation model is similar, containing a bi-coordinated MH_4L^{2+} and a tetra-coordinated MH_2L^+ species and also a hexa-coordinated $M^{III}L$ neutral complex. For M = Ga, the $M^{III}L$ complex should have an hexa-coordination core and a close octahedral structure (see Scheme 2) although, for M = Gd, the complex structure may be distorted due to its usual octa-coordination core, which is completed by the presence of water molecules in the inner coordination sphere (see section Molecular modeling of the Gd complexes below).

Table 1 Stepwise protonation constants (log K_i)[a] and global formation constants[b] and pM[c] values for the Gd^{III} and Ga^{III} complexes of a set of tripodal compounds (T = 25.0 ± 0.1 °C, I = 0.1 M KCl)

Compound	log K_i	(m,h,l)	log β ($Gd_mH_hL_l$)	log β ($Ga_mH_hL_l$)
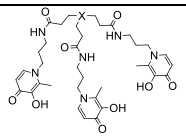 ***H_3L2*** (X = C-NO_2)	9.93(2)	(1,4,1)	37.74(4)	41.52(6)
	9.75(4)	(1,2,1)	30.03(6)	37.60(5)
	9.18(5)	(1,0,1)	21.22(5)	33.15(6)
	4.26(5)			
	3.11(6)			
	2.77(7)	**pM**	**14.3**	**26.2**
H_3L1 (X = N)	9.95[d]	(1,5,1)	42.8[e]	46.70[f]
	9.84[d]	(1,4,1)	39.46[e]	-
	9.09[d]	(1,3,1)	35.69[e]	40.00[f]
	6.77[d]	(1,2,1)	31.16[e]	-
	3.81[d]	(1,1,1)	26.35[e]	38.79[f]
	3.14[d]	(1,0,1)	-	33.34[f]
	2.76[d]	(1,5,2)	65.3[e]	-
		[1,3,2)	52.3[e]	-
		pM	**12.3**	**26.2**
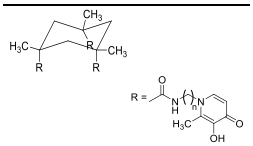 Kemp(PrHP)$_3$[g] n =2	10.07	(1,4,1)	-	41.00
	9.89	(1,2,1)	-	37.62
	9.18			
	3.98			
	3.25			
	2.91	**pM**		**18.4**
Kemp(BuHP)$_3$[g] (n =3)	10.15	(1,4,1)	-	41.78
	9.91	(1,2,1)	-	38.34
	9.21			
	4.05			
	3.38			
	3.10	**pM**		**18.4**

[a] $K_i = [H_iL]/[H_{i-1}L][H]$; [b] $\beta(M_mH_hL_l) = [M_mH_hL_l]/[M]^m[H]^h[L]$; [c] pM value at pH = 7 (pM = -log $[M^{3+}]$, $C_L = 10^{-5}$ M, $C_L/C_M = 10$) ref. 25; [d] ref. 22; [e] ref. 14; [f] ref. 9; [g] ref. 23.

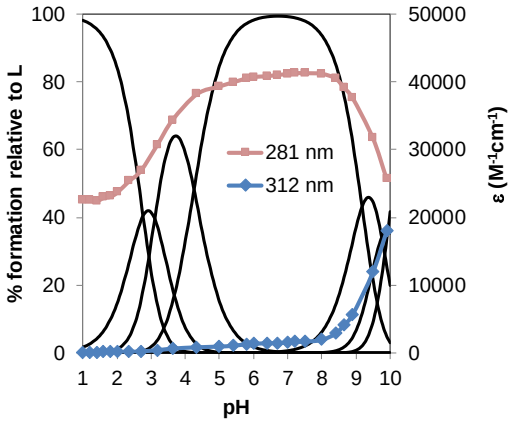

Fig. 3 Species distribution curves of compound H_3**L2** with molar extinction coefficients at the maximum absorption wavelengths (C_L = 5.3 × 10^{-5} M).

From the calculated solution equilibrium model for the metal complexation (below pH 7), the corresponding complex species distribution diagrams along the pH were obtained for selected experimental conditions (see Fig. 4). Analysis of Fig. 4 shows that the Ga^{III} complex formation starts well below pH 2, while the Gd^{III} complexation starts around pH 2. Moreover, the neutral hexa-coordinated $M^{III}L$ species becomes prevalent at pH ca 2.5 and 4.5, for M = Ga and M = Gd, respectively, confirming once more the already expected stronger affinity of compound H_3**L2** for Ga^{III} than for Gd^{III}. Since the concentration of ^{68}Ga used for PET is 10^6 times lower than that used in the performed solution equilibrium studies, species distribution curves for the Ga^{III}/**L2** system were also calculated (Fig. 4 c) under the PET concentration conditions. It can be observed that Ga^{III}**L2** species is predominant above pH 3 and it is predicted that at pH 7, ca 10% of gallium is hydrolyzed (GaH_{-4} species).

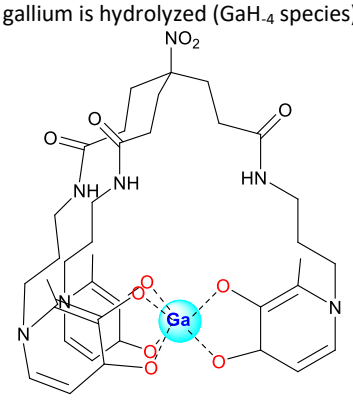

Scheme 2 Structural formula of Ga^{III}-**L2** complex (charges are omitted in Ga (3+) and the deprotonated 3,4-HP moieties [3 x (-1)].

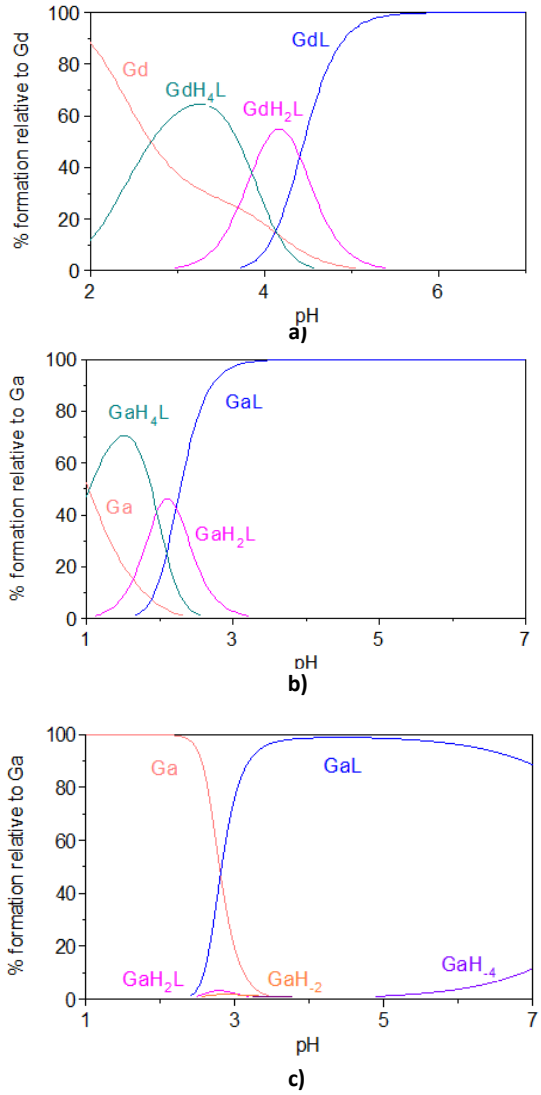

Fig. 4 Species distribution curves for the ligand/metal systems (C_L/C_M = 1): a) Gd^{III}/H_3**L2** (C_{Gd} = 3.2 × 10^{-4} M), b) Ga^{III}/H_3**L2** (C_{Ga} = 5.3 × 10^{-5} M) and c) Ga^{III}/H_3**L2** (C_{Ga} = 5.3 × 10^{-11} M).

Moreover, in order to evaluate whether H_3**L2** is a good ^{68}Ga chelator, it must also be taken in account that this compound is able to complex Fe^{III} and Al^{III} impurities usually present in reagents containing ^{68}Ga. Nevertheless, the *in vivo* performed biodistribution studies (see section below) suggested *in vivo* stability and rapid clearance of the radiolabeled ^{67}Ga chelate.

MALDI-TOF spectra of 1:1 solutions for the Gd^{II}/H_3**L2** (pH = 4.13 and 4.93) and Ga^{III}/H_3**L2** (pH = 3.04 and 4.18) systems confirmed the presence of the hexacoordinated complex species $[GaH\mathbf{L2}]^+$ (*m/z* 836/838, [L2-3H^+ +Ga^{III} +H^+], see Figure S2; unfortunately, for the Gd^{III}/H_3**L2** system it was not possible to find an enough intense m/z signal for the complex to detect the correct isotopic distribution pattern.

Analysis of the data contained in Table 1, namely the pM values (pM = - log $[M^{III}]$, C_L/C_M = 10, C_L = 1 × 10^{-5} M) calculated for pH = 7) allows direct comparison of the metal chelating capacity of H_3**L2** with that

of other analogous tripodal 3,4-HOPO ligands. Both H_3**L2** and H_3**L1** compounds have similar chelating capacities towards Ga^{III}, although H_3**L2** appears to have somehow higher affinity for Gd^{III} than H_3**L1**. Concerning Kemp(PrHP)$_3$ and Kemp(BuHP)$_3$, their much lower chelating capacity towards Ga^{III} can be explained by their lower backbone flexibility as well as by their shorter length arms as compared to compounds H_3**L2** and H_3**L1**, which make more difficult the metal wrapping and lower the complex stability. Other tripodal ligands, such as TREN-Me-3,2-HOPO (pGd = 20.3 at pH 7.4),[26] TRENMAM (pGd = 19.27 at pH 7.4) and TREN-Me-MAM (pGd = 19.03 at pH 7.4), are reported as stronger Gd^{III} chelators since they contain 3,2-HOPO or pyrone moieties that allow a more suitable geometric orientation towards metal complexation.[27]

The remarkable thermodynamic stability of the Ga^{III} complexes with H_3**L1** (a tripodal compound similar to H_3**L2**) was already compared with that of several polydentate aminocarboxylate chelators (e.g. DTPA and EDDA), and it was concluded that this high chelating capacity above pH 4 should prevent competition with endogenous ligands or metals resulting in transchelation or transmetalation.[9] Therefore, when searching for efficient Gd^{III} or Ga^{III} chelators envisaging MRI or PET imaging agents, the development of more flexible tripodal compounds with 3,4-HP moieties seems to be a good research target, due to the diminished drug toxicity induced by metal accumulation in tissues.

Molecular modeling of the Gd complexes

Since it was not possible to obtain good crystals of Gd^{III}**L2** complexes for X-ray diffraction, DFT calculations[18] were carried out in order to get some insight in the molecular structure of this complex, namely to prospect its capacity for enclosing metal-coordinated water molecules, a determinant feature for its magnetic properties. Molecular simulations were carried out with full geometry optimization of **L2**-gadolinium complexes containing one or two coordinated water molecules. Thus, quantum mechanical calculations based on DFT methods, included in the Gaussian 09 program software were used,[19] with the B3LYP hybrid functional[20] and the Stuttgart/Dresden ECP (SDD) basis set.[21] No symmetry constrains were enforced during geometry optimization. The calculations were also performed for one water molecule, by using the same functional and basis set.

The energy-minimized structures, obtained for the 1:1 Gd^{III}**L2** complexes with 1 to 2 coordinating water molecules, are presented in Fig. 5. Both complexes evidence quite similar structures, having the apical NO_2 group directed outside the cavity of the tripodal scaffold. Although in the Gd^{III}**L2**.2H_2O complex the second water molecule appears to be slightly more distant from the metal ion, it still remains in the vicinity of the metal coordination sphere.

From the obtained modeling simulations, the coordination bond distances can be calculated for both structures: Gd-O_{ligand} (2.39(9) Å, average value with standard deviation in parenthesis) and Gd-O_{water} (2.434 Å) for Gd**L2**.1H_2O; Gd-O_{ligand} (2.40(6) Å) and Gd-O_{water} (2.436 and 2.537 Å) for Gd^{III}**L2**.2H_2O. The herein calculated Gd-O_{ligand} bond distances are in good agreement with those previously determined for the out configuration of Gd^{III}**L1**.2H_2O (average 2.42(8) Å)[8] and the experimental X-ray structure of the complex Gd(TREN-Me-3,2-HOPO).2H_2O (average 2.38(3) Å).[26] Concerning the already reported Gd-O_{water} bond distances, the X-ray values obtained for Gd(TREN-Me-3,2-HOPO).2H_2O were 2.446 and 2.436 Å,[26] while those calculated for Gd^{III}**L1**.2H_2O were higher (average 2.58(7) Å).[8] In any case, the values obtained herein for the bond distances between Gd^{III} and either of the water molecules remain in the typical range for complexes with analogous tripodal compounds.

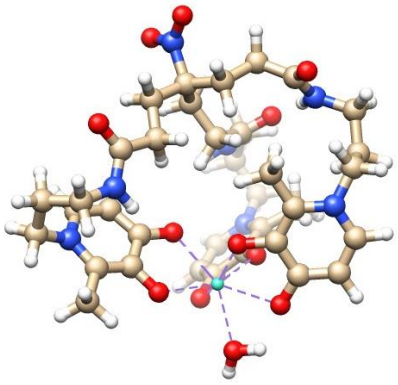

a)

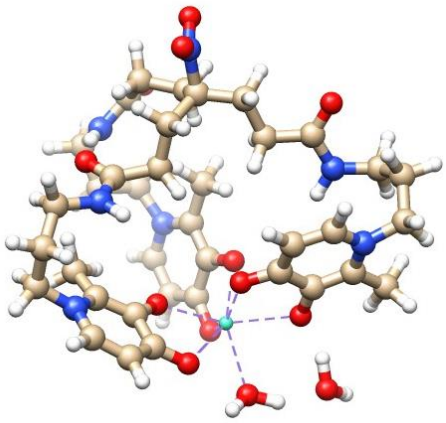

b)

Fig. 5 DFT-minimized structures of 1:1 gadolinium complexes with a) one (Gd^{III}**L2**.H_2O) and b) two (Gd^{III}**L2**.2H_2O) water molecules in the coordination core. Coloring of atoms: Gd (light blue), N (blue), O (red), C (beige) and H (white).

Since complexes Gd^{III}**L2**.1H_2O and Gd^{III}**L2**.2H_2O do not have the same number of atoms, comparison of complex stability was based on the determination of the free energy difference (ΔG = 7.42 kcal/mol) between Gd^{III}**L2**.1H_2O complex plus one water molecule and Gd^{III}**L2**.2H_2O complex. The calculations show that the Gd^{III} complex with two water molecules is more stable than that with one water molecule, in spite of the second water molecule being slightly further apart from the Gd^{III} ion.

Water exchange rate and relaxometric properties of Gd^{III}L2

In order to characterize water exchange rate on the Gd^{III}**L2** chelate, variable temperature ^{17}O NMR measurements were carried out. Given the limited solubility of the complex (~0.5 mM), the paramagnetic ^{17}O chemical shifts could not be determined, therefore only the transverse relaxation rates have been recorded on an aqueous solution of Gd^{III}**L2** ($1/T_2$) and on a diamagnetic reference ($1/T_{2A}$). The temperature dependence of the reduced transverse relaxation rates ($1/T_{2r}$ = ($1/T_2$-$1/T_{2A}$)/P_m, where P_m is the molar

fraction of the coordinated water) is shown in Fig. 6. Above ~300 K, the $1/T_{2r}$ values increase with decreasing temperature, corresponding to a fast exchange regime. Below ~300 K, the trend is different, implying that the system is in a slow water exchange regime. The data have been fitted to the Solomon-Bloembergen-Morgan (SBM) model of paramagnetic nuclear relaxation (see Supporting Information for the equations). The presence of two inner sphere water molecules was assumed, based on the molecular simulations and by analogy to similar HOPO-derivative Gd^{III} complexes, including Gd^{III}**L1**.[8] Some experimental crystal structures are also available in the HOPO family for Gd^{III} or La^{III} complexes.[26,28] The DFT calculations on Gd^{III}**L2** indicate that the two inner sphere water molecules are not equivalent as their distance from the metal ion is different, hence their water exchange rate might also differ. Nevertheless, the ^{17}O NMR data do not allow for distinguishing two separate water exchange rates, therefore the calculated value corresponds to an "effective" rate constant.

The fit of the ^{17}O NMR data yielded the rate (k_{ex}^{298}), the activation enthalpy ($\Delta H^{\neq}$) and entropy ($\Delta S^{\neq}$) of the water exchange, the scalar coupling constant (A/ħ) as well as the parameters describing electron spin relaxation, such as the correlation time for the modulation of the zero-field-splitting (τ_v^{298}), its activation energy (E_v) and the mean-square zero-field splitting energy (Δ^2). These parameters are summarized and compared to those of analogous systems in Table 2.

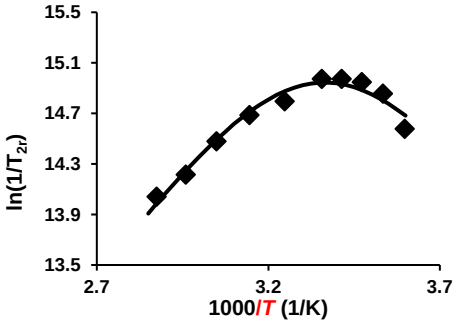

Fig. 6 Temperature (*T*, K) dependence of the ^{17}O reduced transverse relaxation rates (ln $1/T_{2r}$) for Gd^{III}**L2** at 9.4 Tesla (T) (C_{GdL} = 0.45 mmol/kg).

Table 2 Parameters obtained from the analysis of ^{17}O NMR and NMRD data

Parameter	Gd^{III}**L1**[a]	Gd^{III}**L2**	Gd[TREN-Me-3,2-HOPOTAM][b]
k_{ex}^{298} / 10^7 s^{-1} [c]	6.5	0.82±0.11	9.1
$\Delta H^{\ddagger}$ kJ mol^{-1} [c]	18.5	27.7±0.7	7.0
$\Delta S^{\ddagger}$ J $mol^{-1}K^{-1}$ [c]	-33	-20±4	-
$A/\hbar$ / 10^6 rad s^{-1} [c]	-3.2	-3.4±0.2	-3.6
τ_R^{298} / ps [d]	127	τ_g^{298} = 2700±300 τ_l^{298} = 25±5	125
E_r / kJ mol^{-1} [d]	12.0	13±1	-
τ_v^{298} / ps	14[d]	80±15[c]	18
Δ^2 / 10^{20} s^{-2}	3.1[d]	2.1±0.1 [c]	1.1
E_v / kJ mol^{-1}	1.0 [e]	1.0 [e]	-

[a] ref. 8; [b] ref. 29; [c] from the fit of ^{17}O transverse relaxation rates; [d] from the fit of NMRD data; [e] fixed in the fit.

The water exchange rate for Gd^{III}**L2** is almost one order of magnitude lower than for Gd^{III}**L1**, despite the similar coordination environment of the metal ion in the two complexes. On the other hand, the mechanism of the exchange remains associatively activated, as it is indicated by the negative value of the activation entropy, although $\Delta S^{\neq}$ is slightly lower for Gd^{III}**L2** suggesting a less strong associative character of the mechanism. Given the typical coordination numbers of 8 or 9 for Gd^{III}, such associative exchange is indeed expected for an eight-coordinate Gd^{III} chelate. It is also in full accordance with previously studied eight-coordinate HOPO-derivative chelates, for some of which the associative water exchange mechanism was further confirmed by a negative value of the activation volume as well, determined by variable pressure ^{17}O NMR measurements.[29] The considerably slower water exchange on Gd^{III}**L2**, as compared to Gd^{III}**L1**, may be due to their charge difference. In an associatively activated exchange process, the rate-determining step is the entering of the incoming water molecule into the first coordination sphere. While the direct coordination environment of the metal ion is expected to be similar in both complexes, their overall charge is different: the protonation of the apical nitrogen in Gd^{III}**L1** leads to a positive charge, while Gd^{III}**L2** is neutral. Hence, one can argument that the entering of an additional water molecule, which will approach by its oxygen bearing a partial negative charge, in the rate-determining step of the water exchange process can be facilitated by a positive overall charge of the complex. This can lead then to a higher water exchange rate for Gd^{III}**L1** as compared to the neutral Gd^{III}**L2**.

The capacity of a paramagnetic complex to affect water proton relaxation is typically expressed by the proton relaxivity, defined as the increase of the longitudinal proton relaxation rate in the presence of 1 mM concentration of the complex. Higher relaxivity translates to a better MRI efficiency of the system. Proton relaxivities are often recorded as a function of the magnetic field. Such Nuclear Magnetic Relaxation Dispersion (NMRD) profiles are interesting since they provide information on the relaxation mechanisms involved. NMRD profiles on Gd^{III}**L2** were recorded at two different temperatures (25 and 37 °C) between 0.04 and 400 MHz proton Larmor frequency (Fig. 7). These profiles are remarkably different from those previously reported for Gd^{III}**L1**, since the relaxivity hump observed is centered at a much lower frequency, 20 MHz, instead of 80 MHz or above for Gd^{III}**L1**.[8] The maximum relaxivity was centered even at higher frequency (~ 100 MHz) for the Gd^{III} complex of the tris-hydroxymethyl-substituted derivative of TREN-Me-3,2-HOPO.[30] The maximum relaxivity value is also higher for Gd^{III}**L2** (r_1 = 10.5 $mM^{-1}s^{-1}$ at 20 MHz, 25 °C) as compared to Gd^{III}**L1** (r_1 = 8.9 $mM^{-1}s^{-1}$ at 80 MHz, 25 °C). Qualitatively, these differences in the shape of the NMRD profiles are indicative of differences in the rotational motion of the complexes. Thanks also to the presence of two inner sphere water molecules, the relaxivity of Gd^{III}**L2** is remarkably higher than that of clinically used monohydrated Gd^{III}-based contrast agents such as GdDOTA (r_1 = 4.2 $mM^{-1}s^{-1}$ at 20 MHz, 25 °C).

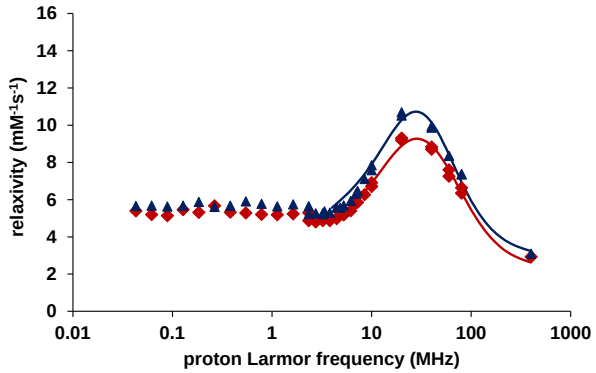

Fig. 7 Proton relaxivities measured for Gd^{III}**L2** at T = 25 °C (▲) and 37 °C (♦) at 0.49 mM concentration. The solid lines represent the fit as explained in the text.

The high-field part of the NMRD profiles (above 3 MHz) for Gd^{III}**L2** was attempted to fit to the usual Solomon-Bloembergen-Morgan (SBM) theory (see Supporting Information for the equations). At these high frequencies, the SBM theory is normally adapted to describe electron spin relaxation and rotation. The relaxivity bump which appears at such low frequency could be reproduced only by considering the Lipari-Szabo approach for the description of the rotational dynamics.[31] This approach is used to describe slowly rotating systems by separating a slow global motion (characterized by a global rotational correlation time, τ_g^{298}) from faster local motions of the Gd-water proton vector (characterized by a local rotational correlation time, τ_l^{298}). An additional parameter, S^2 (between 0 and 1) characterizes the restriction of the local motion with respect to the global one; small or high S^2 values imply, respectively, systems which are flexible or which have restricted local motions. Given its neutrality, the Gd^{III}**L2** complex has a higher tendency to aggregate than Gd^{III}**L1**. As a result, its solubility is limited to sub-mM concentrations, but also, even at the concentration of the NMRD measurements (0.49 mM), some aggregates are already present as evidenced by the form of the NMRD profiles. It should be noted that the relaxivities are well reproducible for the same concentration but decrease by ~5−10% at the maximum of the NMRD curve (at 20 and 40 MHz) when the Gd^{III}**L2** concentration is decreased to half, also evidencing the aggregation effect. In the fit, the water exchange parameters have been fixed to the values obtained from the ^{17}O NMR data, and the global and local rotational correlation times, τ_g^{298} and τ_l^{298} their activation energies, and the electronic relaxation parameters were calculated. A good fit of the NMRD profiles has been achieved with the parameters presented in Table 2 (see ESI for full parameter set). These parameters reproduce well the frequency dependency of the relaxivities, in particular the shape of the high field peak, but it should be noted that they correspond to the aggregation state at a given concentration, thus should not be over-interpreted. This analysis shows first of all that some aggregation is present; it is responsible of the particular form of the NMRD curve (maximum shifted to lower frequencies) and of the higher maximum relaxivity value with respect to Gd^{III}**L1**.

Overall, these ^{17}O NMR and NMRD studies showed that small variations in the ligand chemical structure can have an important impact on the water exchange process and on the relaxation properties of the corresponding Gd^{III} complexes. The charge difference between Gd^{III}**L1** (+1 charge) and Gd^{III}**L2** (neutral) might be the major factor to explain the difference in the water exchange rate and in the aggregation tendency.

Radiolabelling and Biodistribution studies

Radiolabelling of H_3**L2**, was obtained by using the SPECT radionuclide ^{67}Ga due to is longest half life (78.2 h) that allowed to follow the in vivo fate of the complex for 24 h and to its easy availability in our laboratory. For that, ^{67}Ga citrate was added to a ligand solution in acetate buffer pH 5.0 at room temperature. Quality control of the radiolabeled complex was made by ITLC detection. A radiochemical purity (RCP) higher than 98% was obtained.

The biodistribution profile of the ^{67}Ga-**L2** complex was studied in healthy CD-1 female mice (at 30 min, 1 h and 24 h after intravenous injection in the tail vein (see Fig. 8). Overall the radiolabeled complex showed a fast clearance from the blood immediately after administration, primarily through renal excretion, as shown by the high uptakes in the kidneys both at 30 min and at 60 min after injection (5.8 ± 1.1 and 3.7 ± 1.5% I.A./g, respectively) and the high total radioactivity excretion (57.3 ± 9.4, 62.3 ± 2.0 and 88.5 ± 0.8% I.A. at 30 min, 1 h and 24 h, respectively). However, a small contribution from the hepatobiliary tract for the elimination of the ^{67}Ga complex was also observed. At the 24 h time point, besides the uptake by the organs involved in the excretory pathways, liver and especially kidney, no relevant uptake was found in any major organ or tissue. These findings suggest high in vivo stability of the ^{67}Ga-**L2** since the tissue distribution associated to the usual radiochemical impurity species, namely ^{67}Ga-hydroxides and free $^{67}Ga^{3+}$, is well-known and was not observed. Indeed, the presence of free radiometal is related with slow blood clearance, low whole body radioactivity excretion and high bone uptake while radiochemical impurities in colloidal forms, like ^{67}Ga hydroxides $(Ga(OH)_3$ and $Ga(OH)_4^-)$, are mostly taken and cleared by the mononuclear phagocyte system organs which causes high hepatic and splenic uptake that increases overtime and have a long residence time in these organs. Therefore, the fast clearance from bloodstream and rapid washout from main organs of ^{67}Ga-**L2** associated to the low liver and spleen uptakes (2.3 ± 0.9, 1.5 ± 0.6, 0.24 ± 0.01% I.A./g at 0.5, 1 and 24 h, respectively), and (0.7 ± 0.2, 0.5 ± 0.2, 0.10 ± 0.03% I.A./g at 0.5, 1 and 24 h, respectively) led us to conclude that the presence of *in vivo* radiochemical impurities is unlikely. Additionally, the found biodistribution profiles and *in vivo* stability patterns are in agreement with the *in vivo* behavior previously reported for ^{67}Ga complexes with similar hexadentate tripodal ligands.[9,20] A special emphasis must be pointed to the quite high excretion rates found in the presence of this type of ligands, which signify quick elimination of radioactivity from the animal body. The administration of $NTP(PrHP)_3$ (H_3**L1**) leads to a faster clearance from main organs than $Kemp(PrHP)_3$, while **L2** seems to present an intermediate behavior, probably due to the better lipohydrophilic balance and metal affinity of the first two compounds.[22]

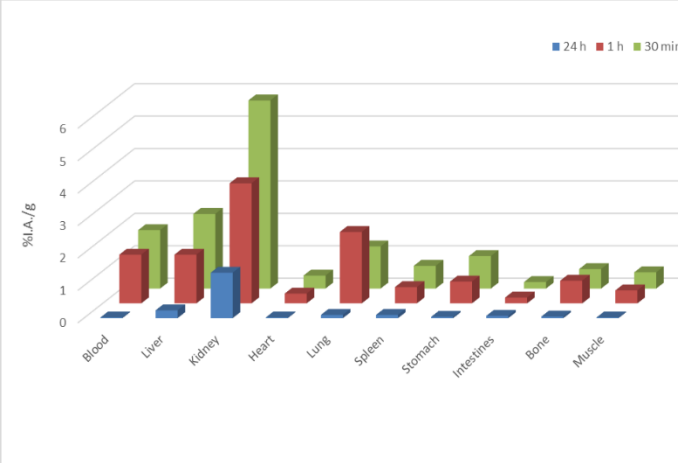

Fig. 8 Biodistribution of ^{67}Ga-**L2** in CD1 mice, expressed as %I.A./g tissue, at 30 min, 1 h and 24 h after intravenous injection (n = 3).

Conclusions

A novel hexadentate ligand (H_3**L2**), containing three 3,4-HOPO moieties attached on tetrahedral carbon core bearing a functionalizable nitro group, was synthesized and studied for its complexation properties with Gd^{III} and Ga^{III}, two (M^{III}) metal ions of great interest in medical imaging. The carbon anchoring scaffold of H_3**L2** intended to improve ligand flexibility, as compared to a previously reported analogue (H_3**L1)** with an amine anchor, to allow for better wrapping of the metal ions and thus stronger metal coordination. Results of solution equilibrium studies showed that H_3**L2** forms 1:1 M/L complexes with high thermodynamic stability (pGd = 14.3 and pGa = 26.2 at pH 7), though with considerable stronger affinity for Ga^{III}. DFT calculations on the structure of the Gd^{III} chelate indicate the presence of two water molecules in the inner coordination sphere. The water exchange rate of Gd^{III}**L2** is one order of magnitude lower than that of Gd^{III}**L1,** which is attributed to their different charge. Indeed, for associatively activated water exchange processes, a positive charge on the complex Gd^{III}**L1** can favor the entering of the incoming water molecule in the rate-determining step. Thanks to the two inner sphere water molecules, Gd^{III}**L2** has remarkably high proton relaxivity, amounting to r_1 = 10.5 $mM^{-1}s^{-1}$ at 20 MHz, 25 °C. The frequency dependence of the proton relaxivities is slightly different from that reported for the Gd^{III}**L1** analogue, suggesting different electron spin relaxation and rotational dynamics. The biodistribution of the radiometal complex [^{67}Ga**L2**] shows that it is mainly excreted through the kidneys and, after 24 h of injection, almost no radiation trace of the complex was found in the organism.

Overall, the above set of important thermodynamic, magnetic and biological properties, evidenced for the complexes of this new tripodal chelator with Ga(III) and Gd(III), suggests **L2** as a promising platform for further anchor extrafunctionalization to promote biotargeting specificity and to improve the lipo-hydrophylic balance of the corresponding metal complexes. This allows for envisaging prospective applications of the corresponding targeted labeled conjugates as MRI and ^{68}Ga-PET diagnostic pharmaceuticals.

Author Contributions

Conceptualization, M.A.S.; methodology, S.C. and E.T.; Software, K.G. and S.C.; Investigation, K.G, K.C., S.C. A.P. L.G. and E.T.; Data Curation, S.C., L.G. and E.T.; Original Draft Preparation, M.A.S., S.C. L.G. and E.T.; Review & Editing, M.A.S., S.C. and E.T.; Supervision, M.A.S., S.C. and E.T. All authors have read and agreed to the published version of the manuscript.

Conflicts of interest

There are no conflicts to declare.

Acknowledgements

The authors from (IST) University of Lisbon are thankful to *Fundação para a Ciência e Tecnologia* (FCT) for financial support to the projects UIDB/00100/2020 and UIDP/00100/2020 and also to the Portuguese NMR (IST-UL Center) and Mass Spectrometry Networks (Node IST-CTN) for providing access to their facilities. We are also thankful to Prof. Luís. F. Veiros for supervision of the molecular modeling studies of the gadolinium complexes and to Dr. Conceição Oliveira for helping in the interpretation of the MALDI-TOF spectra. We also acknowledge the COST Action CA18202, NECTAR, supported by COST (European Cooperation in Science and Technology).

1 A.Y Louie, *Chem. Rev.,* 2010, 110, 3146–3195.
2 J.N. Morrow, E. Tóth, *Inorg. Chem*., 2017, **56**, 6029–6034.
3 J. Wahsner, E.M.Gale, A. Rodríguez-Rodríguez, P. Caravan, *Chem. Rev*., 2019, **119**, 957–1057.
4 D. Cressier, M. Dhilly, T.T.C. Pham, F. Fillesoye, F. Gourand, A. Maïza, A.F. Martins, J.-F. Morfin, C.F.G.C. Geraldes, E.Tóth, L. Barré, *Mol. Imaging Biol*., 2016**, 18**, 334–43.
5 H. Watanabe, M. Ono, S. Iikuni, M. Yoshimura, K. Matsumura, H. Kimura, H. Saji, *Biorg. Med. Chem. Lett.*, 2014, **24**, 4834–4837.
6 F. Bois, C. Noirot, S. Dietemann, I.C. Mainta, T. Zilli, V. Garibotto, M.A. Walter, *Am. J. Nucl. Med. Mol. Imaging*, 2020, **10**, 349-374.
7 A. Datta, K.N. Raymond, *Acc. Chem. Res*., 2009, **42**, 938–947.
8 A.C. Mendonça, A.F. Martins, A. Melchior, S.M. Marques, S. Chaves, S. Villette, S. Petoud, P.L. Zanonato, M. Tolazzi, C.S. Bonnet, E. Tóth, P. Di Bernardo, C.F.G.C. Geraldes, M.A. Santos, *Dalton Trans.*, 2013, **42**, 6046–6057.
9 S. Chaves, A.C. Mendonça, S.M. Marques, A.F. Martins, M.I.M. Prata, A.C. Santos, C.F.G.C. Geraldes, M.A. Santos, *J. Inorg. Biochem.,* 2011, **105**, 31–38.
10 R. Cusnir, C. Imberti, R.C. Hider, P.J. Blower, M.T. Ma, *Int. J. Mol. Sci.,* 2017, **18**, 116.
11 X. Zhou, L.L. Dong, Y. Li, M.C. Cui, L.T. Shen, *Results Chem.,* 2021, **3**, 100240.
12 R. Cappai, K. Chand, J.I. Lachowicz, S. Chaves, L. Gano, G. Crisponi, V.M. Nurchi, M. Peana, M.A. Zoroddu, M.A. Santos, *New J. Chem*., 2018, **42**, 8050–8061.

13 W.L.F. Armarego, D.D. Perrin, *Purification of Laboratory Chemicals*, Butterworth-Heinemann Press, Oxford, 1999.
14 V.M. Nurchi, R. Cappai, K. Chand, S. Chaves, L. Gano, G. Crisponi, M. Peana, M.A. Zoroddu, M.A. Santos, *Dalton Trans.*, 2019, **48**, 16167–16183.
15 F.J.C. Rossotti, H. Rossotti, *J. Chem. Ed.*, 1965, **42**, 375–378.
16 P. Gans, A. Sabatini, A. Vacca, *Talanta,* 1996, **43**, 1739–1753.
17 L. Zékány, I. Nagypál, G. Peintler, PSEQUAD 2001, 501.
18 R.G. Parr, W. Yang, *Density Functional Theory of Atoms and Molecules*, Oxford University Press, New York, 1989.
19 M.J. Frisch, G.W. Trucks, H.B. Schlegel, G.E. Scuseria, M.A. Robb, J.R. Cheeseman, G. Scalmani, V. Barone, B. Mennucci, G.A. Petersson, H. Nakatsuji, M. Caricato, X. Li, H.P. Hratchian, A.F. Izmaylov, J. Bloino, G. Zheng, J.L. Sonnenberg, M. Hada, M. Ehara, K. Toyota, R. Fukuda, J. Hasegawa, M. Ishida, T. Nakajima, Y. Honda, O. Kitao, H. Nakai, T. Vreven, J.A. Montgomery Jr, J.E. Peralta, F. Ogliaro, M. Bearpark, J.J. Heyd, E. Brothers, K.N. Kudin, V.N. Staroverov, T. Keith, R. Kobayashi, J. Normand, K. Raghavachari, A. Rendell, J.C. Burant, S.S. Iyengar, J. Tomasi, M. Cossi, N. Rega, J.M. Millam, M. Klene, J.E. Knox, J.B. Cross, V. Bakken, C. Adamo, J. Jaramillo, R. Gomperts, R.E. Stratmann, O. Yazyev, A.J. Austin, R. Cammi, C. Pomelli, J.W. Ochterski, R.L. Martin, K. Morokuma, V.G. Zakrzewski, G.A. Voth, P. Salvador, J.J. Dannenberg, S. Dapprich,; A.D. Daniels, O. Farkas, J.B. Foresman, J.V. Ortiz, J. Cioslowski, D.J. Fox, Gaussian 09, Revision E.01, Gaussian, Inc., Wallingford CT, 2013.
20 C.W. Bauschlicher, *Chem. Phys. Lett*., 1995, **246**, 40–44.
21 (a) U. Haussermann, M. Dolg, H. Stoll, H. Preuss, P. Schwerdtfeger, R.M. Pitzer, *Mol. Phys.*, 1993, **78**, 1211–1224. (b) W. Kuchle, M. Dolg, H. Stoll, H. Preuss, *J. Chem. Phys.*, 1994, **100**, 7535–7542. (c) T. Leininger, A. Nicklass, H. Stoll, M. Dolg, P. Schwerdtfeger, *J. Chem. Phys.*, 1996, **105**, 1052–1059.
22 S. Chaves, S.M. Marques, A.M.F. Matos, A. Nunes, L. Gano; T. Tuccinardi, A. Martinelli, M.A. Santos, *Chem. Eur. J*., 2010, **16**, 10535–10545.
23 R. Grazina, L. Gano, J. Sebestik, M.A. Santos, *J. Inorg. Biochem.*, 2009, **103**, 262–273.
24 M.T. Beck, I. Nagypal, *Chemistry of complex equilibria*, Ellis Horwood Ltd, Chichester, 1990.
25 K.N. Raymond, C.J. Carrano, *Acc. Chem. Res.*, 1979, **12**, 183–190.
26 J. Xu, S.J. Franklin, D.W. Whisenhunt Jr., K.N. Raymond, *J. Am. Chem. Soc.*, 1995, **117**, 7245–7246.
27 D.T. Puerta, M. Botta, C.J. Jocker, E.J. Werner, S. Avedano, K.N. Raymond, S.M. Cohen, *J. Am. Chem. Soc.*, 2006, **128**, 2222–2223.
28 S.M. Cohen, J. Xu; E. Radkov, K.N. Raymond, M. Botta, A. Barge, S. Aime, *Inorg. Chem.*, 2000, **39**, 5747–5756.
29 M.K. Thompson, M. Botta, G. Nicolle, L. Helm, S. Aime, A.E. Merbach, K.N. Raymond, *J. Am. Chem. Soc.*, 2003, **125**, 14274–14275.
30 S. Hajela, M. Botta, S. Giraudo, J. Xu, K.N. Raymond, S. Aime, *J. Am. Chem. Soc.*, 2000, **122**, 11228–11229.
31 F.A. Dunand, E. Tóth, R. Hollister, A.E. Merbach, *J. Biol. Inorg. Chem*., 2001, **6**, 247–255.